Numerical analysis of breaking waves

Y. Watanabe, H. Saeki
Port and Harbor Engineering Laboratory, Department of Civil Engineering, Hokkaido University, N13 W8, Sapporo 060, Japan

Abstract

Two-dimensional wave motion in a surf zone was numerically solved to obtain temporal and spatial characteristics of the velocity field and energy dissipation, and these results were compared with measurements by the particle image velocimetry. This direct numerical analysis can express splash-up and propagation of a front bore with large vortexes after breaking. The characteristics of vorticity and energy dissipation for a plunging breaker, which vary in a complicated manner with space and time, were also investigated.

1 Introduction

To investigate the mechanisms of sediment transportation in a surf zone, time-averaged fluid velocities, such as return current and nearshore current, or the turbulence field which occurs by impulsive fluid force, have been studied. For the former, the time-averaged velocity distribution can be estimated by using a simple model of time-averaged Reynolds stress (Okayasu et al.[9]), since time-averaged Reynolds stress varies gently in a surf zone. However, it is very difficult to model the latter, as there is complex turbulent field, depending on the type and scale of breaking wave, and the Reynolds stress varies greatly with space and time. Since mean flow and turbulence affects each other, the study of turbulence generated by breaking waves is important to understand the process by which sediment is rolled up and transported onto a sandy coast.

However, it is also difficult to experimentally measure fluid velocity in this region, especially near the front bore, due to the mixture of air bubbles. Sakai et al.[2] simulated fluid motion, including motion in the front bore, in a surf zone by

the SMAC method. Park & Miyata[3] directly solved Navier-Stokes equation for the velocity field at wave breaking as the air and water layer flow, by the marker density technique. These methods, which distinguish the free surface by markers, make the interface obscure, as accuracy of the methods depend on the number of markers in each grid, which leads to numerical diffusion. The cubic-polynomial interpolation (CIP) method is proposed for solving hyperbolic equations by Yabe et al.[4,5]. This method gives stable and less diffusive results, and is especially advantageous for preventing numerical diffusion on the surface.

In this paper, we simulate the two-dimensional velocity field in a surf zone by the CIP method. We were able to express the splash-up and front roller after breaking, and some spatial and temporal characteristics of the energy dissipation in this region were clarified.

2 Numerical Method

Although the validity of the turbulence model, as the eddy viscosity model, has been comfirmed under conditions of a stationary homogeneous turbulent field, excess turbulence diffusion may be induced by this model under conditions of an unsteady flow with a high velocity gradient. Therefore, we should solve the full Navier-Stokes equation in this problem.

In general, the turbulent field should be treated as three-dimensional. However, a two-dimensional wave field is used in this simulation, as it is still expected to investigate characteristics of the splash-up and horizontal roller in a two-dimensional velocity field.

2.1 Computational Procedures

Navier-Stokes equation is used as a governing equation.

$$\frac{D\boldsymbol{u}}{Dt} = -\frac{1}{\rho}\nabla p + \frac{1}{\mathrm{Re}}\nabla^2\boldsymbol{u} + \boldsymbol{g} \tag{1}$$

All variables in equation (1) have been non-dimensionalized with wave celerity (C), water depth (h) and the water density (ρ).

Equation (1) is split into two phases: the non-advection phase and the non-advection phase[6].

Non-advection phase:
$$\frac{\partial\boldsymbol{u}}{\partial t} = -\frac{1}{\rho}\nabla p + \frac{1}{\mathrm{Re}}\nabla^2\boldsymbol{u} + \boldsymbol{g} \tag{2}$$

Advection phase:
$$\frac{D\boldsymbol{u}}{Dt} = 0 \tag{3}$$

Equation (3) in the advection phase is solved by using the intermediate velocities obtained in the non-advection phase. In the non-advection phase, equation (2) discreted by the finite difference method, and is separately solved by dividing

one time step into two procedures.

$$\frac{\boldsymbol{u}'^{n+1/2} - \boldsymbol{u}'^{n}}{\Delta t} = -\frac{1}{\rho}\nabla p'^{n+1/2} + \boldsymbol{g} \tag{4}$$

$$\frac{\boldsymbol{u}'^{n+1} - \boldsymbol{u}'^{n+1/2}}{\Delta t} = \frac{1}{\mathrm{Re}}\nabla^2 \boldsymbol{u}'^{n+1/2} \tag{5}$$

Taking the divergence of equation (4), a Poisson equation for the pressure is expressed as

$$\nabla^2 p'^{n+1/2} = \rho\frac{\nabla\cdot\boldsymbol{u}'^{n}}{\Delta t} \,. \tag{6}$$

The pressure can be obtained simply by the MAC algorithm from equation (6). The Crank-Nicolson method, which has second order accuracy, is used to evaluate the velocities in the non-advection phase at a new time step.

In the advection phase, equation (3) is solved by the CIP method proposed by Yabe et al.[4,5]. The CIP method is outlined bellow.

A physical function $f(\xi, \eta)$ and its derivatives in a rectangular grid with the vertex nodes (i,j), (i+1,j), (i,j+1) and (i+1,j+1) are interpolated between each node as follows.

$$f_{ij} = a_1\xi^3 + a_2\xi^2\eta + a_3\xi^2 + a_4\xi\eta + \frac{\partial f_{ij}}{\partial x}\xi + a_5\eta^3 + a_6\eta^2\xi + a_7\eta^2 + \frac{\partial f_{ij}}{\partial y}\eta + f_{ij} \tag{7}$$

$$\frac{\partial f_{ij}}{\partial x} = 3a_1\xi^2 + 2a_2\xi\eta + 2a_3\xi + a_4\eta + a_6\eta^2 + \frac{\partial f_{ij}}{\partial x} \tag{8}$$

$$\frac{\partial f_{ij}}{\partial y} = 3a_5\eta^2 + 2a_6\xi\eta + 2a_7\eta + a_4\xi + a_2\xi^2 + \frac{\partial f_{ij}}{\partial y} \tag{9}$$

ξ and η are the distances from the node (i,j) in the directions of (i+1,j) and (i,j+1), respectively. Since $f(\xi, \eta)$ is continuous between each node, a_1 to a_7 are determined as follows.

$$a_1 = \left(2\left(f_{ij} - f_{i+1\,j}\right) + \left(\frac{\partial f_{ij}}{\partial x} + \frac{\partial f_{i+1\,j}}{\partial x}\right)\Delta x\right)\Big/\Delta x^3$$

$$a_2 = \left(f_{ij} - f_{ij+1} - f_{i+1\,j} + f_{i+1\,j+1} + \left(\frac{\partial f_{ij}}{\partial x} - \frac{\partial f_{ij+1}}{\partial x}\right)\Delta x\right)\Big/\Delta x^2\Delta y$$

$$a_3 = \left(3\left(f_{i+1\,j} - f_{ij}\right) - \left(2\frac{\partial f_{ij}}{\partial x} + \frac{\partial f_{i+1\,j}}{\partial y}\right)\Delta x\right)\Big/\Delta x^2$$

$$a_4 = \left(-f_{ij} + f_{ij+1} + f_{i+1\,j} - f_{i+1\,j+1} + \left(-\frac{\partial f_{ij}}{\partial x} + \frac{\partial f_{ij+1}}{\partial x}\right)\Delta x + \left(-\frac{\partial f_{ij}}{\partial y} + \frac{\partial f_{i+1\,j}}{\partial y}\right)\Delta y\right)\Big/\Delta x\Delta y$$

$$a_5 = \left(2\left(f_{ij} - f_{ij+1}\right) + \left(\frac{\partial f_{ij}}{\partial y} + \frac{\partial f_{ij+1}}{\partial y}\right)\Delta y\right)\Big/\Delta y^3$$

$$a_6 = \left(f_{ij} - f_{ij+1} - f_{i+1j} + f_{i+1j+1} + \left(\frac{\partial f_{ij}}{\partial y} - \frac{\partial f_{i+1j}}{\partial y} \right) \Delta y \right) \Big/ \Delta x \Delta y^2$$

$$a_7 = \left(3\left(f_{ij+1} - f_{ij} \right) - \left(2\frac{\partial f_{ij}}{\partial y} + \frac{\partial f_{ij+1}}{\partial y} \right) \Delta y \right) \Big/ \Delta y^2$$

We can assume that the physical function f_{ij} at the node (i,j) after a small interval Δt is transported from the point located at $\xi = -u\Delta t$, $\eta = -v\Delta t$. It means that the physical function $f(x,y,t+\Delta t)$ equals $f'(x-u\Delta t, y-v\Delta t, t)$ in the numerical procedure if Δt is sufficiently small (See Figure 1). The above constants, a_1-a_7 correspond to the constants at the node (i,j) when the horizontal velocity $u<0$ and the vertical velocity $v<0$. Thus, if $f(x,y,t) = \boldsymbol{u}$, substantial differential equation (3) can be evaluated by equations (7)-(9) with constants, a_1-a_7 which depend on the direction of velocity at the node. A free surface can also be updated by the same procedure, as will be described next section.

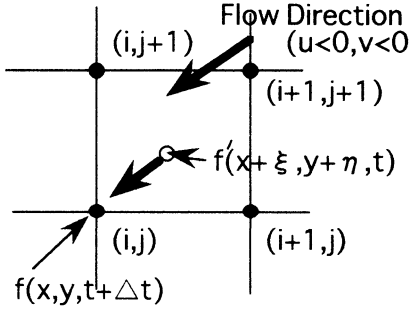

Figure 1: Evaluation of advection term

2.2 Free Surface Condition

The density function method is used to distinguish between water and air. The density function ρ_f indicates 1 in a grid with filled fluid and 0 in a grid without fluid. If ρ_f takes an intermediate value ($0<\rho_f<1$), both condition exist in the grid. The free surface is defined as that located at the point where $\rho_f = 0.5$. ρ_f at all grids is updated by

$$\frac{D\rho_f}{Dt} = 0. \tag{10}$$

At the free surface, it can be regarded as a kinematic boundary condition. Substantial differential equation (10) is also calculated by the CIP method as equation (3). Although by using the density function method, the free surface is easily obscured by numerical diffusion, this defect can be offset by introducing the CIP method, which has a high level of accuracy.

Ignoring viscous and surface-tension at the free surface, the dynamic boundary condition is

$$p=0. \tag{11}$$

This surface boundary condition can be approximately satisfied by using the irregular star method[10] for equation (6).

2.3 Boundary Conditions

We use two types of numerical wave makers as the inflow boundary condition. One is based on small amplitude wave theory and used for numerical tests. The other can generate second-order cnoidal waves for the simulation of breaking waves.

Sommerfeld's radiation condition has generally been used for a numerical wave flume as an open boundary condition. However, we use a simple no-normal gradient condition for velocities since the wave energy is sufficiently dissipated by breaking on the open boundary near the shore line.

A non-slip condition is introduced as the bottom boundary condition.

3 Particle Image Velocimetry

To confirm the validity of our numerical analysis for fluid motion in a surf zone, the numerical results must be compared with experimental results of the instantaneous fluid velocity distribution of a breaking wave. However, it is very difficult to measure fluid velocity in a plunging jet and turbulent bore after breaking due to mixing with air bubbles.

Thus, we investigated fluid velocity by particle image velocimetry[7,8] (PIV). This method estimates fluid velocities from video images which record the movement of markers mixed in the wave flume. In this method, the following spatio-temporal correlation of some frames are first calculated.

$$C(x+\Delta x, t+t') = \frac{\int \left(f(x,t)-\overline{f(x)}\right)\left(f(x+\Delta x, t+t')-\overline{f(x)}\right)dt}{\left[\int \left(f(x,t)-\overline{f(x)}\right)^2 dt \int \left(f(x+\Delta x, t+t')-\overline{f(x)}\right)^2 dt\right]^{1/2}} \qquad (12)$$

$\triangle x$ and t' denote the distance between the pixels of the particle image and lag time, respectively. $f(x,t)$ denotes the function of brightness and a bar means the average of $f(x,t)$.

Assuming the velocity field is locally stationary, the fluid velocities can be estimated by the following fundamental definition.

$$u = \Delta x / t'_{\max} \qquad (13)$$

where t'_{max} is the lag time for the maximum correlation value among given frames.

In the experiments, we used white markers with a specific gravity of 1.005 and diameter of 2 mm, and a high speed video camera which can take 250 frames per sec. The brightness of the particle images were digitized into a 256 gray scale with a resolution of 10 pixels/mm. The noise in image data was removed by a Gaussian filter. The results measured by PIV had 80% accuracy if the pixel had a

correlation of greater than 0.8.

4 Results

4.1 Numerical Test

Figure 2 shows a comparison between the numerical results and the theoretical results by small amplitude wave theory under conditions where the non-dimensional wave height (H/h) and wave length (L/h) are 0.0625 and 1.25, respectively. The abscissa is the distance from the numerical wave maker and the ordinate is the non-dimensional horizontal (a) and vertical (b) velocity. The bold line and thin line represent the numerical results and the analytical solutions at each depth, respectively. A good agreement between the numerical and theoretical results, can be seen in these figures, confirming the validity of the present numerical analysis.

4.2 Numerical Analysis of Breaking Waves

The vorticity distributions at plunging point are shown in Figure 3 for the cases where the non-dimensional wave height (H/h) and wave length (L/h) are

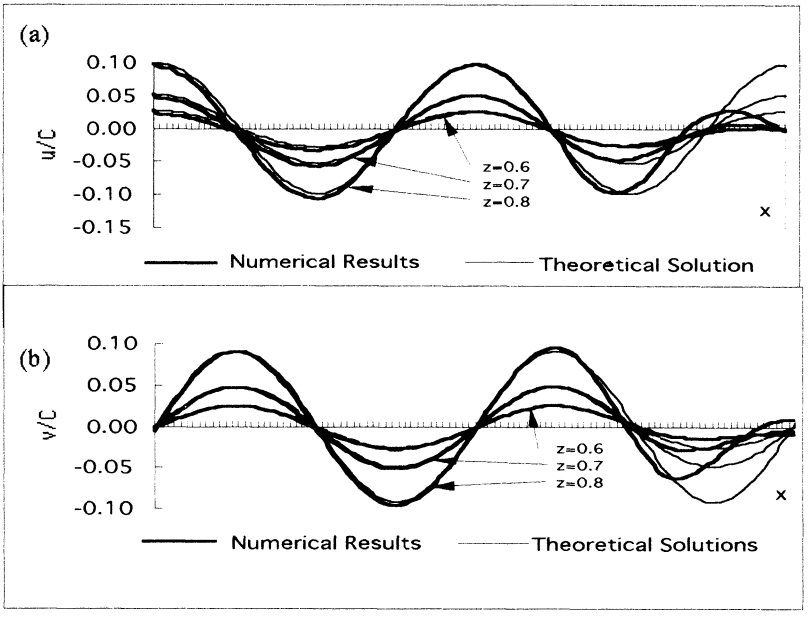

Figure 2: Comparisons between the numerical results and the theoretical results for (a) horizontal velocity and (b) vertical velocity

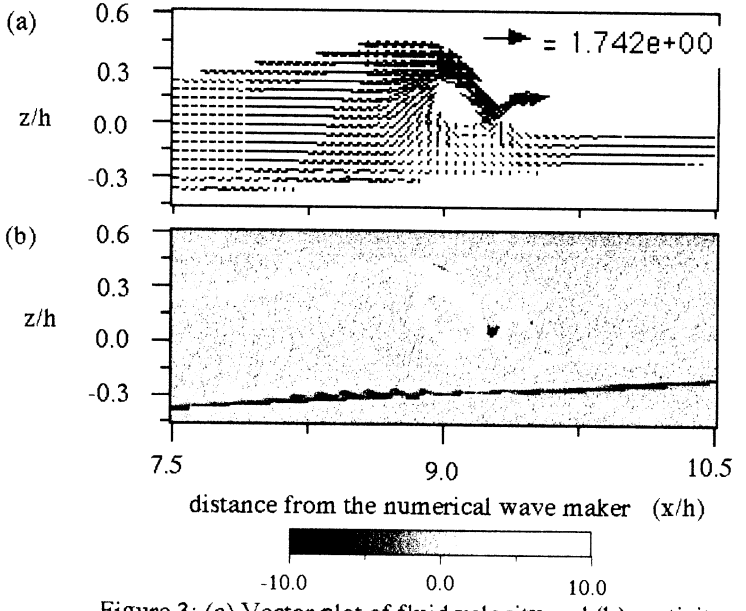

Figure 3: (a) Vector plot of fluid velocity and (b) vorticity distribution at splashing (bottom slope; 1:15)

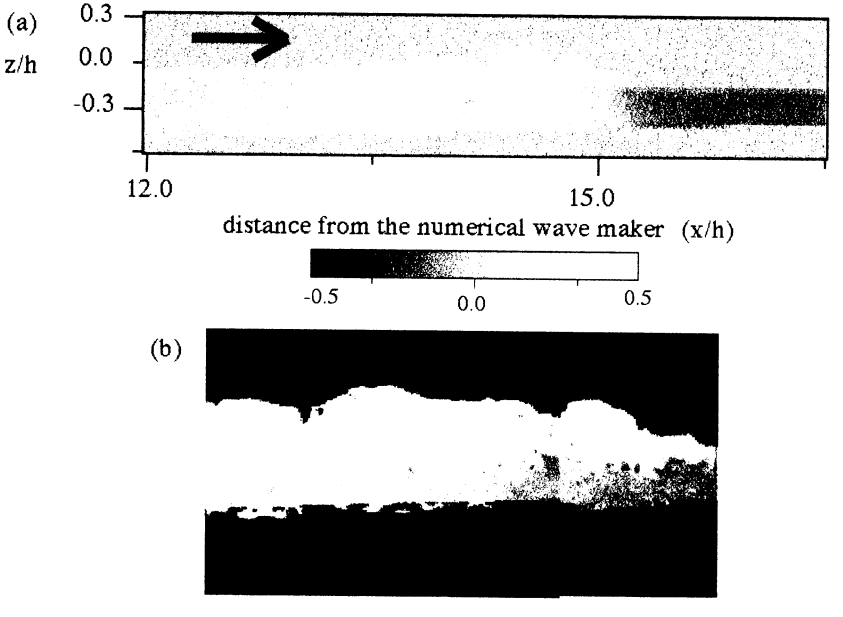

Figure 4: Horizontal velocity distribution after breaking. (a) numerical result (b)experimental result measured by PIV (bottom slope; 1:30)

0.41 and 11.5, respectively. The bottom slope is 1:15. It can be seen that the plunging jet with a high velocity rebounds on undisturbed water and the splash-up commences from this plunging point, and high vorticity occurs around the plunging point. Since the rotaion with same direction exists on both side of the plunging point, strong shear arises between these vortex motions, and negative vorticity is generated by this high shear.

Figure 4 shows the horizontal velocity distribution of the numerical results and the distribution measured by PIV when the bore front propagates after breaking for the case where the wave period is 2.4 sec, breaking wave height is 14 cm, breaking water depth is 15 cm, and the bottom slope is 1:30. The numerical results are similar to the experimental results by PIV for the velocity distributions and the profile of the free surface. Thus, the validity of the present simulation is also confirmed for the fluid motion after breaking in this way.

Figure 5 shows the distribution of vorticity (a) and energy dissipation (b) for the same conditions as in Figure 4. Large vortexes occurring through the splash-up cycles can be seen in Figure (a). In Figure (b), it can be seen that the wave energy is dissipated mainly on the part between large vortexes generated by each plunging, because of high shear between them. It should be noted that a

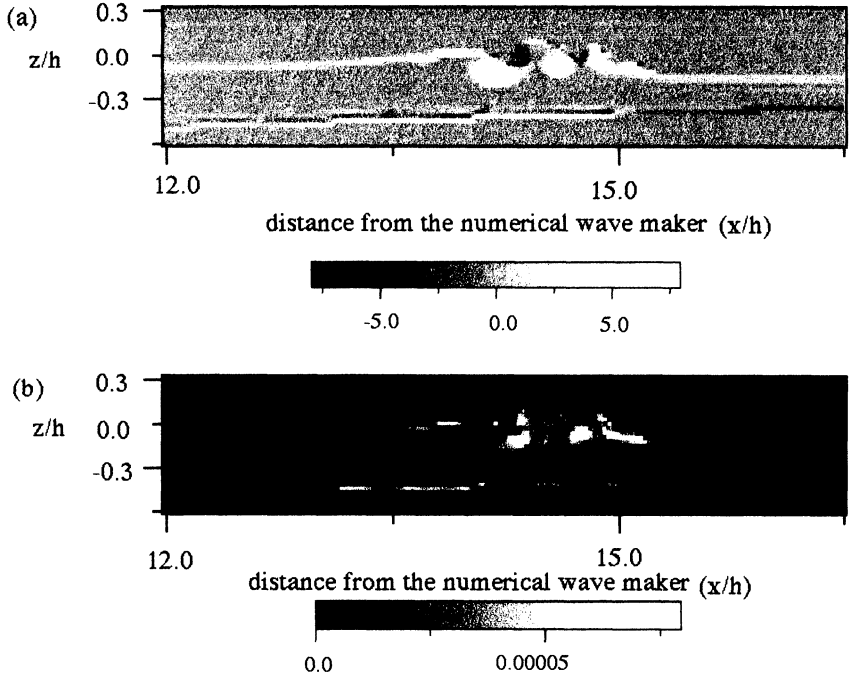

Figure 5: (a) vorticity distribution and (b) energy distribution after breaking (bottom slope; 1:30)

large energy loss occurs near the front bore where shear acts between the plunging jet and the undisturbed water with the opposite horizontal velocity to the velocity of front bore. Therefore, it is expected that a mean flow, such as a return current, affects the process of wave decay. Further investigation of the spatial and temporal characteristics of fluid motion is needed to understand turbulent field in a surf zone.

Figure 6 shows the spatial and temporal relationship of energy dissipation integrated over depth. The abscissa and ordinate represent the distance from the numerical wave maker and time after breaking, respectively. Intensity of energy dissipation is not large before the first plunging point, as it is occured only in a wave boundary layer. Then, energy dissipation impulsively increases near the plunging point. It is can be seen that two parts with a large dissipation exist in region (II), because of the difference between the velocity propagating the front bore and the velocity transported the large vortex under the free surface, as in Figure 5. This process is repeated through the splash-up cycles until the wave energy dissipates sufficiently (region (III)).

5 Conclusions

Direct numerical analysis was used to investigate the details of the fluid motion in a surf zone, and the validity of the numerical analysis was confirmed by a comparison to experimental results measured by PIV.

The splash-up cycles and the front bore propagating with large vortexes could be expressed well in this simulation.

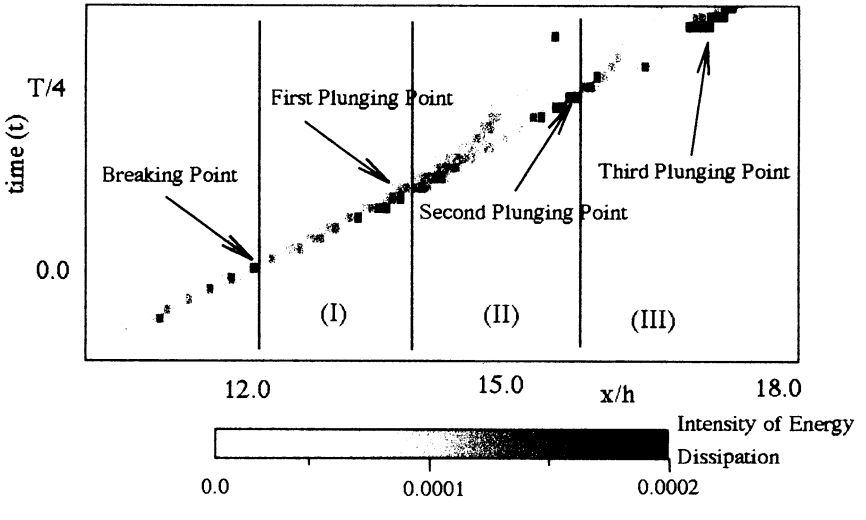

Figure 6: Spatial and temporal relationship of energy dissipation integrated over depth (bottom slope; 1:30)

We investigated the characteristics of production, transportation and decay of the vorticity and the energy dissipation after breaking. Further investigation is needed to evaluate turbulent field closely concerned with rolling up and transportation of sediments.

This numerical method has sufficient level of accuracy and numerical stability for estimating fluid motion which is very non-linear .

Acknowledgements

This study was supported by Grant-in-Aids for Scientific Research (Grant-in-Aids for JSPS Fellows) from the Ministry of Education, Science, Sports and Culture of Japan.

References

1. D. H. Pregrine, Breaking Waves On Beaches, Annual Review of Fluid Mechanics, 1983, Vol. 15, pp. 149-178.
2. T. Sakai, T. Mizutani, H. Tanaka, Y. Tada, Vortex Formation in Plunging Breaker, Proceedings of the International Conference on Coastal Engineering, 1986, pp. 711-723.
3. Jong-Chun Park , Hideki Miyata, Numerical Simulation of the Non-linear Free-Surface Flow Caused by Breaking Waves, FED-Vol. 181, Free-Surface Turbulence, ASME, 1994, pp. 155-168
4. T. Yabe & T. Aoki, A Universal Solver for Hyperbolic Equations by Cubic-Polynomial Interpolation I. One-Dimensional Solver, Computer Physics Communications, 1991, Vol. 66, pp. 219-232
5. T. Yabe, T. Ishikawa, P. Y. Wang, T. Aoki, Y. Kadota, F. Ikeda, A Universal Solver for Hyperbolic Equations by Cubic-Polynomial Interpolation II. Two- and Three-Dimensional Solvers, Computer Physics Communications, 1991, Vol. 66, pp. 233-242.
6. Takashi Yabe & Pei-Yuan Wang, Unified Numerical Procedure for Compressible and Incompressible Fluid, Journal of The Physical Society of Japan, 1991, pp. 2105-2108.
7. Yasunori Watanabe & Hiroshi Saeki, Experimental Study on the Fluid Motion in a Surf Zone by Particle Image Velocimetry, Proceedings of Coastal Engineering, JSCE, vol. 42, 1995, pp. 116-120. (in Japanese)
8. Ronald J. Adrian, Particle-Imaging Techniques for Experimental Fluid Mechanics, Annual Review of Fluid Mechanics, 1991, Vol. 23, pp. 261-304.
9. Akio Okayasu, Tomoya Shibayama, Kiyoshi Horikawa, Vertical Variation of Undertow in the Surf Zone, Proceedings of the International Conference on Coastal Engineering, 1988, pp. 478-491.
10. Chan. R. O. C. & Street. R. L., A Computer Study of Finite Amplitude Water Waves, J. Computational Physics, 1970, vol. 6, pp. 68-94.